



# CNT coating and anchoring beads enhance interfacial adhesion in fiber composites

Sabyasachi Ghosh<sup>\*</sup>, Israel Greenfeld, H. Daniel Wagner<sup>\*</sup>

Department of Molecular Chemistry and Materials Science, Weizmann Institute of Science, Rehovot 76100, Israel

## ARTICLE INFO

### Keywords:

Coated composites  
SWCNT anchored epoxy beads  
Interface  
Mechanical and other functional properties

## ABSTRACT

The fiber-matrix interface is a critical component in fiber composites, affecting both their strength and toughness. In this study, glass fibers were treated with thin coating of CNT bundles, creating a strong scaffold using evaporation-driven deposition. Epoxy beads were applied to the coating, implementing the Plateau-Rayleigh liquid instability phenomenon. The coated and beaded fibers were embedded in epoxy matrix and subjected to pullout tests, yielding a significant increase of 140% in strength and 400% in toughness, compared to untreated fibers. Electron microscopy and 3D micro-CT imaging elucidated the improvement mechanisms, including strengthening and toughening of the fiber-matrix interphase by the scaffold and anchoring of the epoxy beads. Composites reinforced by such fibers should potentially lead to significant enhancement of simultaneously both strength and toughness. Similarly, the mechanical and electrical properties of flexible functional composites can be enhanced by weaving the coated and beaded fibers into a smart fabric.

## 1. Introduction

High-strength and lightweight materials have long been sought after in various research sectors, including the development of safe and fuel-efficient airplanes and the building of huge architectural projects [1–4]. Engineering structures require both strength and toughness (damage tolerance), but in most materials, the two are mutually incompatible [5]. Composites made of Fiber Reinforced Polymer (FRP) are among the most useful and elegant materials of the twenty-first century. Their durability and integrity in diverse service environments are dependent on the fiber, polymer matrix, and the interface/interphase between them [6].

Diverse techniques have been explored and applied to increase the strength and fracture toughness of fiber composites, including altering hard thermoset polymers with ductile thermoplastic polymers and rubber, integrating various fibers into the matrix material to create a hybrid fiber composite, employing large diameter fibers, coating the fibers periodically before embedding them into matrices, interlacing a strong strip between plies of laminated composites, and lowering matrix shrinkage stress [7–11]. Several studies investigated the chemical alteration of the fiber interface via coupling agents to enhance the composite [12–14], but the improvement of one feature is frequently accompanied by the degradation of the other. Generally, minute

modification to interfacial properties in the microscale domain correlates with an enhancement of the macro-composites' bulk characteristics. Thus, structural design of the fiber-matrix interface is a viable strategy for obtaining the desired balance of strength and toughness.

Surface coating of fibrous reinforcements with carbon nanotubes (CNTs) for improving the mechanical and physical properties of composites and endowing the composite with multifunctional properties has raised the interest of scientists over the last decade. Carbon nanotubes (CNTs), a novel member of the fullerene family, have generated much interest among scientists ever since their discovery in 1991 [15]. Theoretically, a single-wall carbon nanotube (SWCNT) is a hollow cylinder created by rolling up a graphene sheet, predicted to have exceptionally high tensile strength [16–19]. SWCNTs have outstanding physical, electrical, mechanical, and optical capabilities that may lead to a wide range of promising applications. Indeed, CNT-modification of epoxy matrix composites improves mechanical properties, such as interlaminar shear strength and impact resistance [20,21]. The use of nanocomponents such as graphene, WS<sub>2</sub>, and CNTs as reinforcing materials is still confined to the lab scale [22–24] because of technical challenges associated with their dispersion and alignment in matrices and on fiber surfaces.

Different methods, including dip coating, spray coating, and electrophoretic deposition (EPD) of CNTs, can be used to graft CNTs onto

<sup>\*</sup> Corresponding authors.

E-mail addresses: [sabyasachi.ghosh40@gmail.com](mailto:sabyasachi.ghosh40@gmail.com) (S. Ghosh), [daniel.wagner@weizmann.ac.il](mailto:daniel.wagner@weizmann.ac.il) (H. Daniel Wagner).

<https://doi.org/10.1016/j.compositesa.2023.107427>

Received 7 November 2022; Received in revised form 22 December 2022; Accepted 4 January 2023

Available online 6 January 2023

1359-835X/© 2023 Elsevier Ltd. All rights reserved.

glass fibers [25–27]. These methods are scalable and simple to implement, but achieving uniformity and thickness in the deposited CNTs is difficult. Some studies have concentrated on improving the interfacial characteristics of fiber composites by employing the EPD process for coating carbon fibers or fabric with a thick layer of CNTs [28–30]. However, only a few studies have attempted to apply a thin coating of CNTs onto a single glass fiber such that the interfacial region would be strengthened without affecting the fiber's intrinsic features [31,32]. CNTs densification (with surfactants like sodium dodecyl sulfate, SDS) and polymer impregnation have also been used to improve the mechanical, electrical, and thermal characteristics of CNT-based composites [33–35] and can be applied by the technique of evaporation-driven solvent coatings [36,37] (also known as evaporation-driven self-assembly).

A different approach to strengthening the fiber–matrix interface is to add mechanical obstacles serving as geometric locks for the fiber in the matrix. For example, applying polymer beads onto the fiber prior to its embedment in the matrix has proven to improve both the strength and toughness of composites, as demonstrated by extensive fiber pullout and fragmentation experiments [11,38,39]. However, to our knowledge, combining fiber coating and mechanical interlocking in a hybrid composite has never been attempted.

In the present study, we integrated two such techniques in a model glass fiber composite: (i) coating of the fibers by SWCNT bundles (b-SWCNTs), applied by evaporation-driven deposition, and (ii) adding epoxy beads (E-beads) on the fibers, applied by the Plateau-Rayleigh instability. To investigate the structural performance of this hybrid

structure, four configurations were tested by fiber pullout tests: pristine fibers, coated fibers, beaded fibers, and coated + beaded fibers. The pullout force and displacement were obtained, demonstrating that the standalone configurations of coated or beaded fibers each improved both their strength and toughness compared to the configuration with the pristine fibers, whereas the combination of coating and beading yielded the highest performance. The hybrid configuration was characterized by three dimensional (3D) micro-CT imaging and analysis, showing consistent coating and beading. The four configurations' effective interfacial strength was calculated from the experimental results, and substantiated by theoretical modeling of the interface using the Cottrell-Kelly-Tyson method [40–42]. In addition, the application of the standalone coated and beaded fibers in flexible composites, for example, by weaving the fibers in the fabric, is described and analyzed.

## 2. Experimental

### 2.1. Raw materials

E-glass fibers were collected from S139 (Vetrotex International Saint-Gobain), with an average diameter of 18.0–18.5  $\mu\text{m}$ . The epoxy system (EP828-Bisphenol-A diglycidyl ether and EPC304-polyetheramine hardener) was obtained from Polymer Gvulot Ltd., Israel. Single Wall Carbon Nanotubes (SWCNTs,  $\geq 95\%$  purity, specific surface area  $\geq 700\text{ m}^2/\text{g}$ , G/D ratio:  $\geq 20$ , melting point 3652–3697  $^\circ\text{C}$ , median length 1  $\mu\text{m}$ , mass density 1.7  $\text{gm}/\text{cm}^3$ , and diameter  $\sim 1\text{ nm}$ ) and Sodium Dodecyl Sulphate (SDS,  $>98.5\%$  GC) were supplied by Sigma

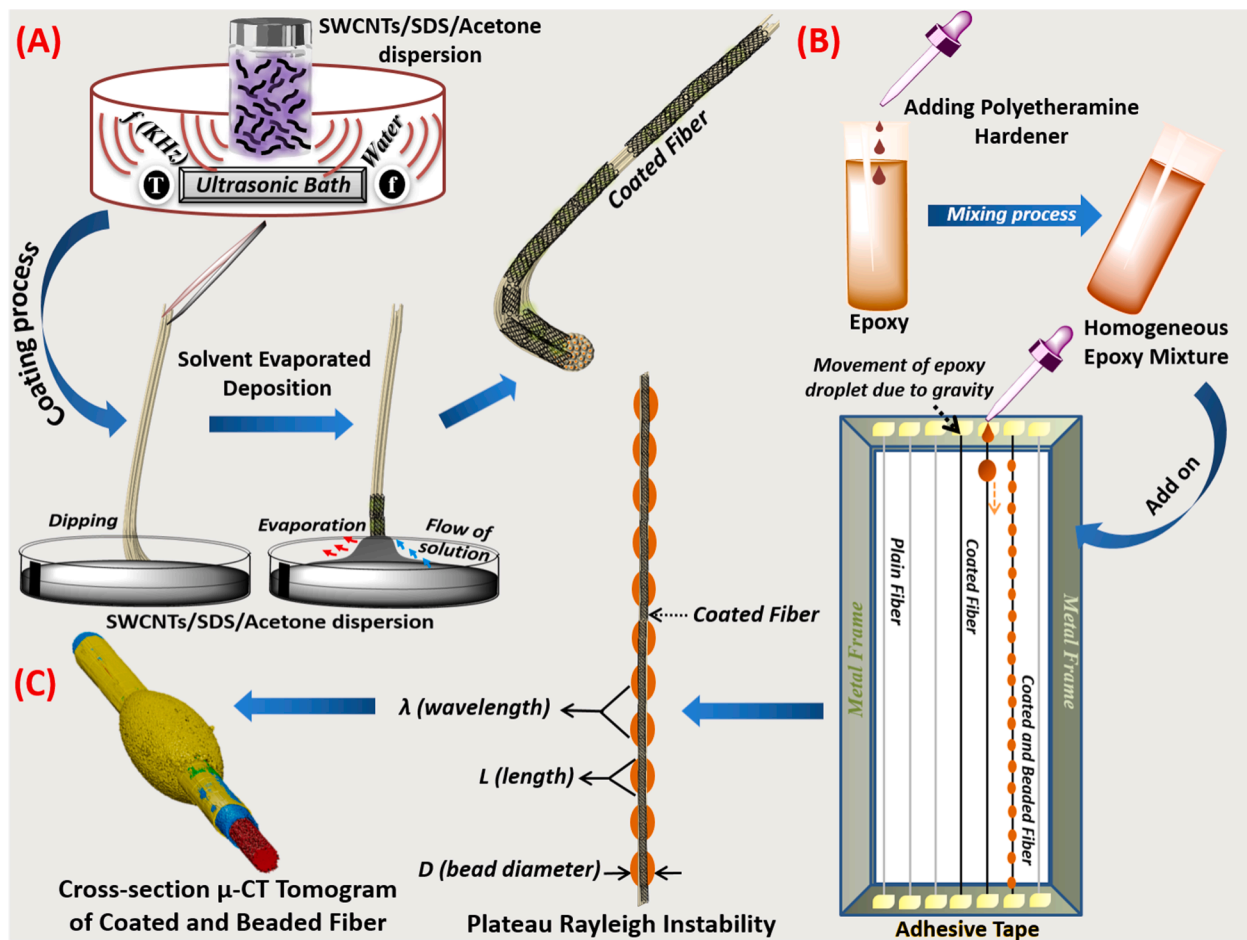


**Fig. 1.** Schematic illustration of self-assembled SWCNTs deposited on fibers and formation of epoxy beads. (A) SWCNT coating of the fiber. (B) Preparation of homogeneous epoxy/hardener mixture. (C) An epoxy droplet is placed on a fiber of diameter ( $d$ ) and allowed to glide down the fiber (both coated and non-coated), forming a thin layer that splits spontaneously into beads with length ( $L$ ) and wavelength ( $\lambda$ ) that are evenly spaced apart.

Aldrich USA.

## 2.2. Deposition of b-SWCNTs and epoxy beads on fibers

Self-assembled b-SWCNTs/fibers were prepared by the “solvent evaporated deposition” method (Fig. 1). 5 mg of SWCNTs were dispersed in acetone (100 mL), and the mixture was sonicated for 30 min. A minimal quantity of SDS (0.25 mg) was added to the mixture and further sonicated for 30 min to obtain a fine dispersion of the SWCNTs within the acetone. The glass fibers were submerged in acetone for 1 h, followed by drying at 80 °C to ensure the removal of impurities and unwanted interactions. The fibers were dipped into the SWCNTs solution cast in a petri-dish, and the solvent evaporation directed a flow of CNT-rich solution towards the fiber, depositing the CNTs on the fiber. The coated fibers were placed in a drying oven at 60 °C for 6 h to eliminate the stresses of solvents. The coated fibers were taken out from the petri-dish, gently stretched, and glued to our laboratory-prepared metal frame using masking tapes. Bisphenol-A diglycidyl ether and polyetheramine hardener were used to create the resin for the epoxy beads. In order to achieve a homogeneous epoxy/hardener mixture free of air bubbles, resin and hardener were typically combined at a weight ratio of 100:42 within a centrifugal mixer employing deaeration capabilities (Thinky ARE-250 CE).

Finally, a drop of epoxy was poured on the coated fibers, which were glued to the metal frame, using a micropipette. The drop was let to fall along the fiber under gravity. The process lasted for 5–7 min, resulting in a thin layer of epoxy with beads on the fiber surface, implementing the Plateau-Rayleigh instability phenomenon. The b-SWCNTs coated and epoxy-beaded fibers were moved to the laboratory oven and cured at 100 °C for 6 h with continuous hot air circulation.

For the purpose of tuning the beads anchoring effect, the bead dimensions (diameter  $D$ , length  $L$  and wavelength  $\lambda$ ) are controlled by the size of the initial drop placed on the fiber. When the drop flows down the fiber by gravity, it coats the fiber by a layer of liquid epoxy that breaks into droplets as a result of the Plateau-Rayleigh instability. The bead dimensions are determined by the thickness of the liquid layer. A more viscous resin and a larger initial drop would result in thicker coating and will form larger beads, and vice versa. Alternatively, the liquid layer can be created by using dip coating, in which the fibers are drawn from a reservoir of liquid epoxy, and the layer thickness is determined by controlling the drawing velocity [11].

## 2.3. Characterization

### 2.3.1. Morphological study

The morphological measurements of different fibers were investigated by scanning electron microscopy (SEM-Zeiss, Sigma-500) with a thin layer of Pd/Ag and a 5 kV acceleration voltage for 2 min, optical microscopy with POM, Nikon, and micro-CT scan measurements with XRadia (microXCT-400, Pleasanton, CA, USA), applying 40 kV and 200  $\mu$ A high-resolution scans.

### 2.3.2. Thermo-gravimetric analysis

TGA was performed to evaluate coating fractions of SWCNTs and SDS on coated and beaded fibers using SDT Q600, TA instruments, at a heating range between 50 °C and 900 °C at a 10 °C/min heating rate, under nitrogen environment.

### 2.3.3. Volume fraction analysis of the b-SWCNTs coating

The b-SWCNTs coating scaffold volume fraction ( $V_{sc}$ ) was measured via the weight fraction of b-SWCNTs extracted from TGA analysis. The total volume of the b-SWCNTs in the scaffold was  $v_{sc} = \frac{m_{sc}}{\rho_{sc}}$ , and the overall scaffold volume was that of a hollow cylinder,  $v_t = \frac{\pi}{4} (D_t^2 - D_f^2) L$ . Therefore

$$V_{sc} = \frac{v_{sc}}{v_t} = \frac{m_{sc}/\rho_{sc}}{\frac{\pi}{4} (D_t^2 - D_f^2) L} \quad (1)$$

where  $m_{sc}$  and  $\rho_{sc}$  are the SWCNTs weight calculated from TGA analysis and SWCNTs density (1.7 g cm<sup>-3</sup>), respectively.  $D_t$ ,  $D_f$ , and  $L$  are the scaffold's external diameter, the fiber diameter, and the TGA sample length, respectively. Likewise, the volume fraction of the SDS surfactant ( $V_s$ ) was calculated using its weight (from TGA analysis) and density (i. e., 1.01 g cm<sup>-3</sup>). The remaining porosity prior to epoxy impregnation, equivalent to the matrix volume fraction in the scaffold, is calculated by

$$\text{porosity} = Vm = 1 - \frac{v_{sc} + v_s}{v_t} \quad (2)$$

### 2.3.4. Fiber pullout test

The interface of fibers with a single bead at their end (both coated and non-coated) and fibers without beads (both coated and non-coated) was investigated through single-fiber pullout test measurements, detailed below.

**2.3.4.1. Sample preparation for the pullout test.** After preparing the fibers as described in experimental Section 2.2, end-beaded fibers were prepared by cutting a long multiple-beaded fiber with a scalpel. The fibers were cut such that the beads were in close proximity to the end of the fiber fragment. Cutting was performed under optical microscopy. Each fiber was dipped into the liquid epoxy (i.e., epoxy: hardener –100:42) using a laboratory-designed heating device consisting of a rotating platform, a heating component, and two equilateral micro-calipers. The liquid epoxy was poured into a metal screw cap that could be fitted to the heating device, ensuring suitable heat distribution. The horizontal micro-calipers and rotating platforms were used for proper fiber positioning. The role of the vertical micro-caliper was to control the dipping length into the epoxy mixture, equivalent to the embedded length ( $L_e$ ). Once the fiber was embedded into the liquid epoxy within the heating platform, it was kept there for 30 min at 100 °C. This allowed holding the fiber in the middle of the epoxy-filled screw cap. Finally, the screw cap (accommodated with an epoxy mixture and the fiber) was moved into the laboratory oven for a full curing cycle for 5 h 30 min at 100 °C (the pre-stage epoxy was partially cured at 100 °C for 30 min during the embedding process to avoid fiber shifting).

**2.3.4.2. Pullout test.** The single fiber pullout test (Fig. 2) was conducted using a piezo-actuator (Physik Instrument GmbH, Germany), load cell (Kistler, Switzerland) and voltage amplifier. The measured force was calibrated within 0–80 N and crosshead movement range of 180  $\mu$ m. The screw cap with the embedded fiber was tied to the load cell. The free end part of the fiber was fixed to the actuator with cyanoacrylate glue (CN, Tokyo Measuring Instruments Laboratory, Japan). The fibers free length was maintained within the range of 50–70  $\mu$ m. This glue was stiff enough when dried out and held the fiber end within the actuator when the pullout test was running. The rate of the pullout measurements was fixed at 1  $\mu$ m s<sup>-1</sup>.

### 2.3.5. Tensile test

The mechanical performance of standalone fibers (both beaded and non-beaded, coated and non-coated) was studied and calculated by an Instron 5965 universal testing system (UK) using a 10 N load cell with a crosshead speed of 1 mm min<sup>-1</sup> and a gauge length of 10 mm. An optical Nikon OPTIPHOT-2 Microscope with a 5580CP-C-OH camera was used for scanning the fiber displacement during the tensile test. A plastic card frame with Poxipol glue was used to support the fiber on the load cell with a pair of fiber clamps. Prior to testing, both side edges of the plastic frame were cut out for effective measurements of the fiber only (inset of Fig. 9A).

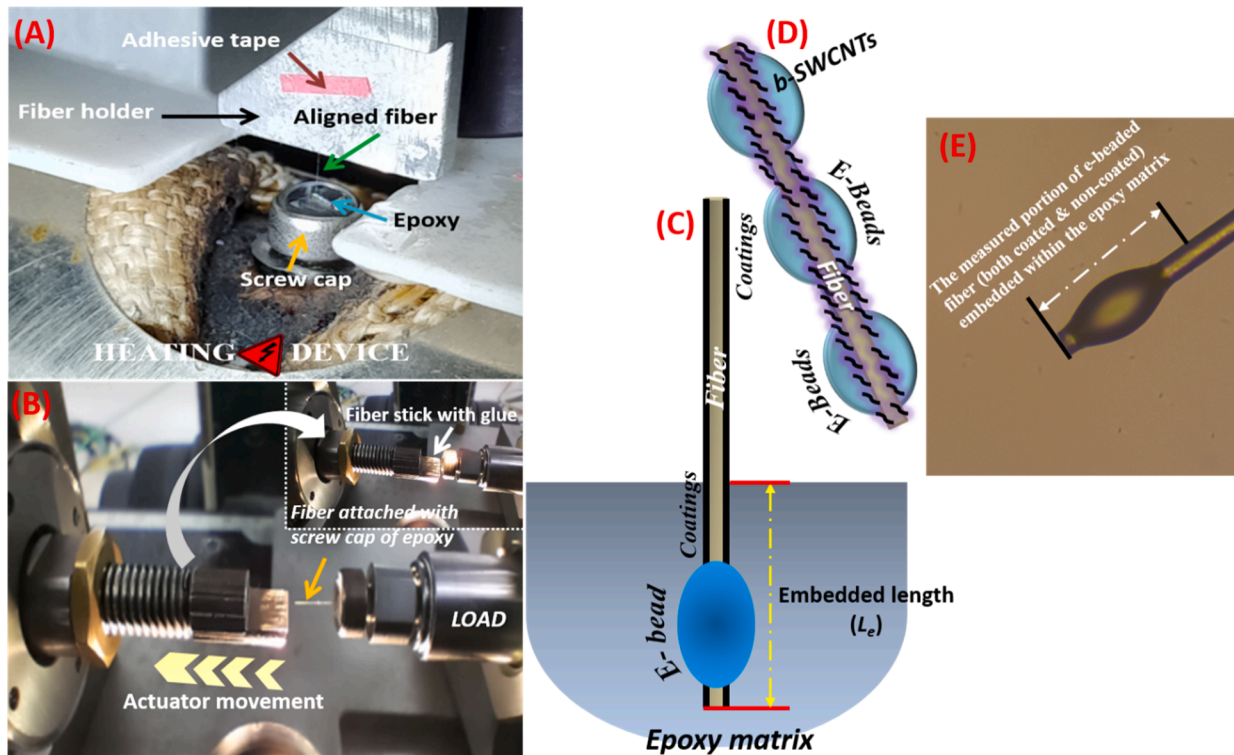


**Fig. 2.** (A) Sample preparation scheme for the pullout test; (B) Fiber attachment with glue and actuator movement for single fiber pullout tests; (C) Pullout sample schematic showing the E-bead at the fiber end with the embedded length  $L_e$  in the epoxy matrix; (D) Schematic arrangements of the prepared fibers; (E) The beaded fiber (for both coated and non-coated) is sliced under an optical microscope to create a bead at the fiber's end. A single bead is encased in an epoxy matrix.

### 2.3.6. Current-voltage (*I-V*) test

Current response measurements were carried out by a Cryogenic Probe Station (Lakeshore TTPX) under ambient conditions. It was conducted across the junction of the fiber surface using a sub-femtoamp source meter (Keithley 6430).

## 3. Results and discussion

### 3.1. Coating and beading conformation

Three different characterizations were performed to analyze the morphological background of the fibers under various treatments: optical microscopy (OM), scanning electron microscopy (SEM), and 3D micro-computed tomography ( $\mu$ -CT) scanning. Fig. S1 depicts the digital and optical images of pristine fibers and fibers after coating and beading. After coating with SWCNTs, the fibers' surface became rough, and the coating layers were securely attached (Fig. 3A). Fig. 3(B-C) shows E-beads deposition on the fiber surface. The fractured surface of different fibers illustrates the densification of SWCNTs within the epoxy matrix (discussed in the next section). The E-beads arrangement is uniformly sized and spaced, with a fairly smooth appearance, whereas prior to beading the surface of the fibers was rough in nature. The average fiber diameter after SWCNTs deposition for 6 h was calculated at around 21.5  $\mu\text{m}$ , larger than the pristine fiber (18.5  $\mu\text{m}$ ), indicating that the coating layers had an approximate thickness of ca. 1.5  $\mu\text{m}$ . The beads' diameter lies at 46.6 ( $\pm 3.6$ )  $\mu\text{m}$ , with corresponding bead length of 78.2 ( $\pm 10.6$ )  $\mu\text{m}$  and wavelength of 140 ( $\pm 40$ )  $\mu\text{m}$ . The deposited SWCNTs were randomly oriented, and a minimal amount of SDS helped achieve homogeneous deposition and attachment of dense SWCNTs or bundled SWCNTs (b-SWCNTs) on the fiber surface.

The SDS acted as a soft template for the SWCNTs scaffolding, and acetone helped wet the microstructure of the SWCNT arrays in the deposition treatment. After placing the glass fibers within the solution and subsequent drying, the SWCNTs appeared to form a dense bundles

structure (b-SWCNTs) on the fiber surface due to both van der Waals interactions and ionic charges on the SWCNTs surfaces, enhanced by the random attachment of SDS (Fig. 4(A-B)) [43]. The SDS induced dispersion of individual hydrophobic SWCNTs by contributing anionic surface charges within the solution and densifying the SWCNTs through capillary forces by acetone penetration into the SWCNTs structure voids. The distribution of SDS was random, and SWCNTs densification was achieved through the attraction of opposite charge clusters [44,45].

Acetone evaporated from the fiber backbone as the fibers were dried under submerged conditions, increasing the densification of bundles (b-SWCNTs) on the fiber surface (Fig. 4C). The approximate b-SWCNTs diameters ranged between 20 and 30 nm (Fig. 4D). During the epoxy beading on the coated fiber surface, the epoxy penetrated the voids in the b-SWCNTs scaffold, achieving high micromechanical interlocking, van der Waals attraction, and ionic bonding that enabled efficient load transfer to the b-SWCNTs from the epoxy bead interface. See schematic illustration of the plausible mechanism in Fig. 4B.

We extended our characterization to three-dimensional micro-computed tomography ( $\mu$ -CT) scanning measurements to obtain the coating characteristics in a three-dimensional (3D) domain. It is a non-destructive experimental technique for displaying the 3D interior microstructure of the sample under experiment. The 3D micrograph of the pristine glass fiber is presented in Fig. 5A, and the cross-sectional micrographs of the coated b-SWCNTs and deposited E-beads are shown in Fig. 5(B-D). The cross sections were measured at two different locations: the bead center and outside the bead. 2D raw micrographs of the coated fiber with and without beads under different intensity variations are illustrated in Fig. S2. After reconstruction of the 2D micrographs in the XRadia software, we constructed 3D micrographs of the coated and beaded fiber, and slice view resolution was measured by Avizo software (VSG). The color-mapping was recorded for the core fiber (red), coatings (both outside the bead, denoted by the blue color and in the bead center, marked in green), and E-beads (denoted by the yellow color).

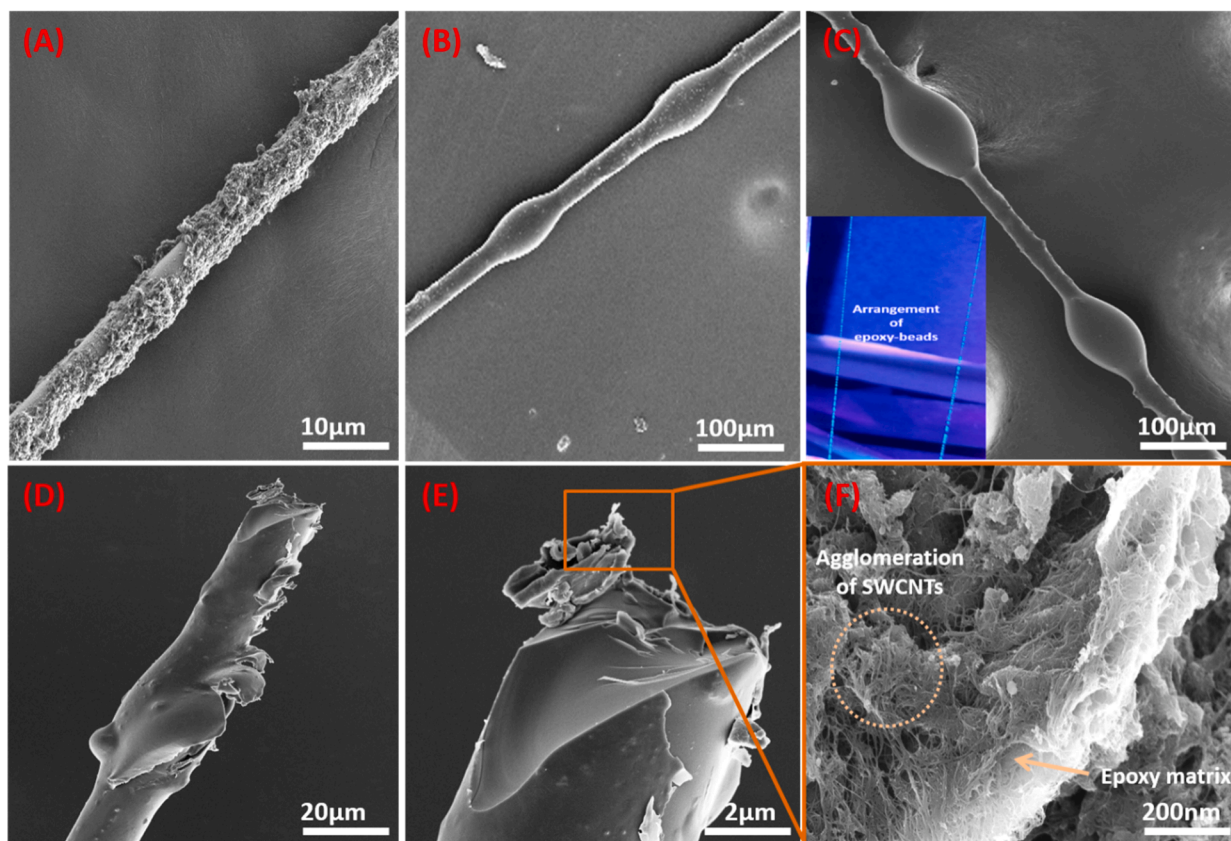


**Fig. 3.** SEM images of (A) SWCNTs coated fiber; (B-C) SWCNTs coated and epoxy beaded fiber; the inset depicts an eye visualization of photo-luminescent (slightly added fluorescent pigment (GEINNOVA) with epoxy) epoxy beads on a glass fiber; (D-E) Fractured (under liquid nitrogen) coated and beaded fibers; (F) A conformation of SWCNT scaffold and epoxy matrix on the fiber surface.

To further explore the coating arrangements of the SWCNT scaffold, we performed a segmental study. The coating thickness variation through the segmental analysis was calculated and is presented in Fig. 5E. In the cross-sectional measurements, we cut the fiber inside the bead (Centre zero (0) position and Slide No. 531) and outside (both the right and left sides w.r.t the bead) to obtain measurements of the coating layer on the fiber surface. The segmental study demonstrated that the coating was uniform in the micro dimension and had an approximate thickness of 1.5  $\mu\text{m}$ . The  $\mu\text{-CT}$  analysis was in agreement with the SEM images (Fig. 3(A-C)), confirming that the glass fiber surfaces were fully covered by roughened SWCNTs (the scaffold) and smoothed E-beads. The coated and beaded fiber was obtained from 987 slides with a corresponding diameter of  $\sim 22.6 \mu\text{m}$  (with a thin epoxy coating of  $\sim 1.1 \mu\text{m}$  in the region without the bead). The coated fibers clearly marked the boundary of the fiber and coating region, and the CT micrographs confirm that fibers and b-SWCNTs were closely bound to each other with the epoxy anchoring beads. The 3D homogeneous architecture of the SWCNTs scaffold on the fiber surface improved the fiber-matrix interface, consequently enhancing the strength and toughness of the coated and beaded fibers (discussed in the next section).

### 3.2. Pullout force and work and effective interfacial strength

A crucial component of fiber composites is the fiber-matrix interfacial domain, as it is the medium through which loads are transferred from the matrix to the fiber. Therefore, pullout tests were executed to analyze the effect of E-beads and b-SWCNT coating on the fiber interfacial strength, compared to the interfacial strength of pristine fibers. In each test, the fiber end was embedded within the epoxy matrix at a length of  $90 \pm 3 \mu\text{m}$  (recorded in Supporting Information Movie 1). The fiber pullout technique is useful for the fiber-matrix interface shear

strength estimation [46]. The embedding method and actuator/load movement for the single fiber pullout tests are presented in Fig. 2. The force vs displacement was recorded during pullout for plain, beaded, coated, and both coated and beaded fibers, as presented in Fig. 6(A-B).

The pullout of the pristine fibers exhibited an elastic-plastic displacement range of  $\sim 5\text{--}15 \mu\text{m}$  and a maximum force of 0.18 N, after which the force dropped sharply, and the fibers pulled out completely. The elastic-plastic displacement range for the beaded fibers lay between  $\sim 10\text{--}20 \mu\text{m}$ , and the maximum force was 0.26 N, higher than the virgin fiber (without beads). The elastic-plastic displacement range for the b-SWCNTs coated fibers was similar to the beaded fibers (length of  $\sim 10\text{--}20 \mu\text{m}$ ), and the maximum force was 0.37 N. The coated and beaded fibers had a maximum elastic-plastic displacement range of  $\sim 40\text{--}50 \mu\text{m}$ , approximately twice the range of the coated and beaded fibers separately. The maximum force was 0.44 N. The pullout work was calculated via integrating the area under the force vs displacement curves of the plain fiber, fiber with bead, coated fiber and coated fiber with bead. These values are plotted in Fig. 6(C-D) and summarized in Table 1. The pullout was accompanied by debonding at the fiber-matrix interface (for both coated and non-coated cases), and the interfacial strength could be derived from the maximum force. Generally, a steep stress drop was observed for all prepared fibers due to fiber debonding from the matrix phase through a long friction segment, which continued until complete pullout.

These results demonstrate that the b-SWCNTs coating significantly improves both maximum force and displacement during fiber pullout, implying a significant improvement in both interfacial strength and toughness. The beaded fibers also demonstrate an improvement in these parameters, in agreement with our previous studies [11,38], but not as significant as the coating effect. Most notably, the individual contributions of coating and beading add up in the coated + beaded fibers,

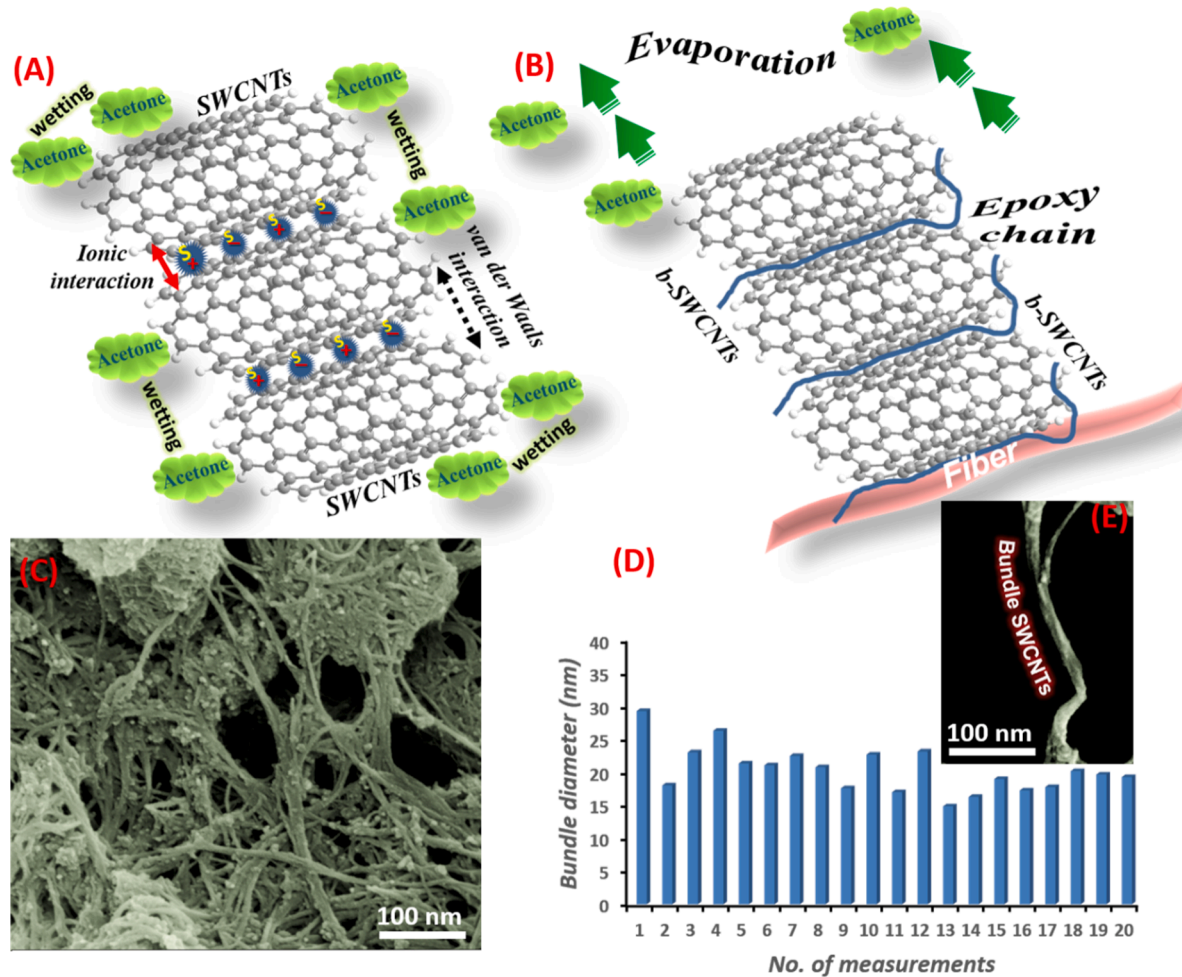


**Fig. 4.** Schematic representation of SWCNTs wetting and b-SWCNTs bundling. (A) The Acetone/SDS solution is added to the freestanding SWCNTs, followed by sonication before drying. SWCNTs become denser due to surface attraction (van der Waals and ionic interactions); (B) Schematic illustration of bundled SWCNTs and epoxy penetration. The acetone evaporation also occurs on the fiber surface during drying; (C) SEM micrograph of b-SWCNTs formation; (D) The range of bundle diameters. The inset depicts a single bundle collected by SEM.

implying that the physical mechanisms governing each configuration are different, and, therefore, their effects are cumulative. Furthermore, the improvement in interfacial strength is accompanied by a simultaneous improvement in toughness, not easily achievable otherwise.

The Cottrell Kelly Tyson (CKT)-based classical expression [41,42] was used for the calculation of the effective interfacial shear strength ( $\tau$ ):

$$\tau = \frac{F_{max}}{\pi d L_e} \quad (3)$$

where  $F_{max}$  is the maximum pullout force,  $d$  is the measured fiber diameter, and  $L_e$  is the embedding length of each fiber (defined in Fig. 2C). The value of  $d$  is the same for all configurations, i.e., 18.5  $\mu\text{m}$ , equal to the fiber diameter. For the pristine fiber,  $\tau_{fiber}$  was calculated at around 34.4 MPa. For the beaded fiber (no coating),  $\tau_{beaded\ fiber}$  was calculated at approximately 48.4 MPa, whereas  $\tau_{coated\ fiber}$  was calculated at  $\sim 68.5$  MPa. Finally, for the combined coated and beaded fiber,  $\tau_{coated\ and\ beaded\ fiber}$  was measured at about 82.7 MPa. The results demonstrate an improvement of  $\sim 200\%$ , attributed to the coating, and an improvement of  $\sim 240\%$  attributed to combined coating and beading, compared to the pristine fibers, constituting a truly significant improvement.

The fiber–matrix interfacial region is a key area of fiber composites, because the external load is transferred from the matrix to the fiber through that interface. During the pullout test, the longitudinal stress induced by the matrix on the bead was converted to radial pressure by

the bead slope, which propagated through the bead and coating towards the fiber interface, consequently generating significant friction that enhanced the interfacial strength [39]. At the same time, the b-SWCNTs deposited on the fiber and impregnated by the epoxy reinforced the interface zone and significantly increased the bonding to the fiber. Thus, the interfacial shear strength was enhanced by two independent mechanisms, high friction and strong bonding, which added up in the coated + beaded fibers, as indeed observed in the pullout tests (Fig. S3). The coating on the fibers also likely improved stress relaxation by eliminating residual stress and reducing internal stresses originating from the fiber coating and bead matrix interface [47].

As noted, our observations demonstrated an enhancement in toughness, indicated by the increase in pullout work, which coincided with the enhancement in the shear strength. Here, as well, the interfacial mechanisms of beading and coating acted separately, adding up in the coated + beaded fibers. The high friction generated by the bead provided shear stress that prevailed over a long displacement (see Fig. 6(C–D)). At the same time, the coating increased energy absorption by the pullout of CNTs from the coating matrix during plastic deformation [48]. The pullout work data of the coated + beaded fibers exhibited more scattering than the other fiber configurations, most probably due to cumulative variations in the beads' diameter (due to the rough surface of the deposited b-SWCNTs) and the coating thickness and density (see Fig. 5E).

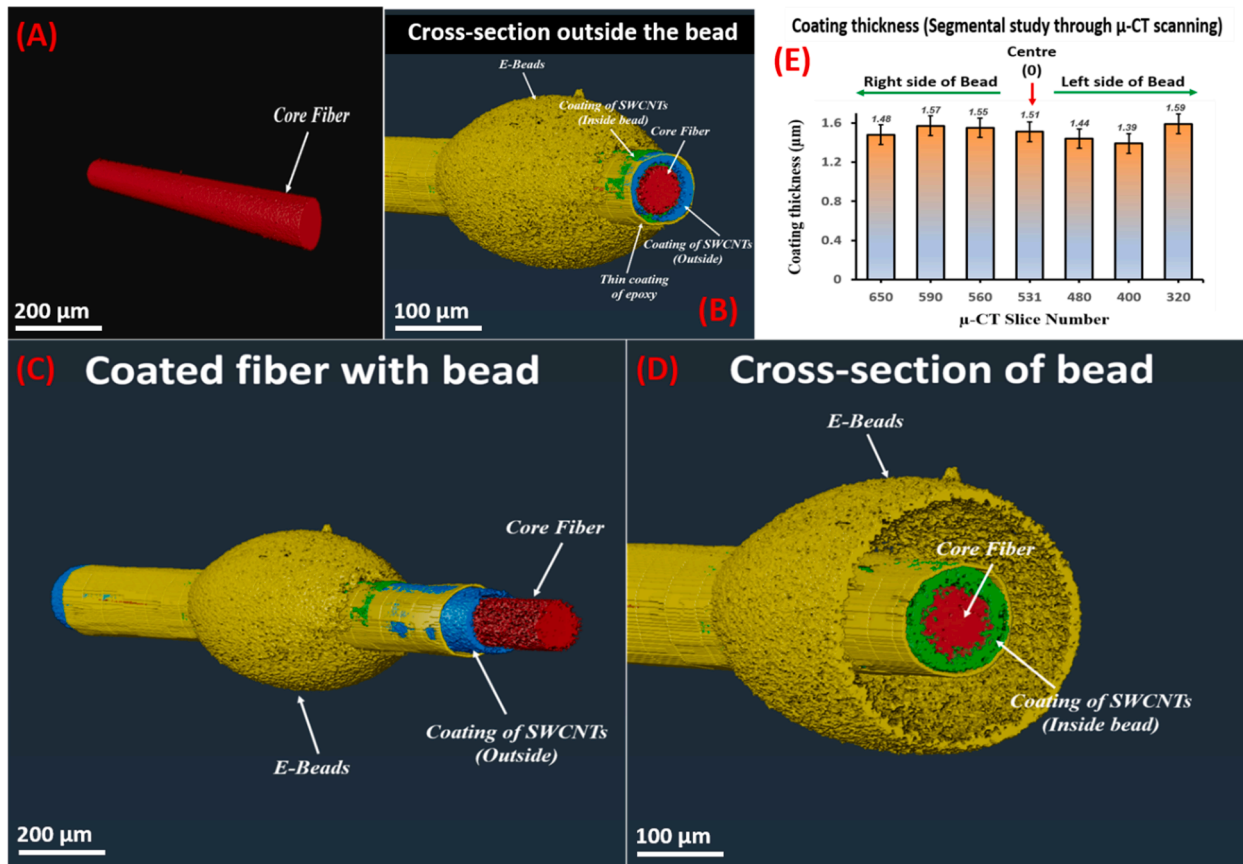


Fig. 5.  $\mu$ -CT images of (A) Normal glass fiber; (B) Cross-sectional image outside the bead; (C) Full 3D image of a coated fiber with a bead; (D) Cross-sectional image through the bead; note: image processing ‘removed’ some material from inside the bead, making it look inadvertently hollow; (E) Coating thickness (average) at different locations (i.e. slice numbers) along the specimen obtained by  $\mu$ -CT segmental study.

### 3.3. Failure analysis of fiber pullout

A micro-dimensional “mechanical interlocking” phenomenon was recorded by the SEM micrographs after the pullout test of the coated and beaded fiber. As shown in Fig. 7 (A-B), the b-SWCNTs were entwined in the coating, acting as “anchors” for the fibers’ reinforcement, while the SDS helped achieve good CNTs dispersion on the fiber surfaces. During the pullout test, the fibers pulled out completely without breaking, whereas the E-beads remained in the epoxy matrix. No epoxy residue was present on the fiber surface. However, clear traces of CNTs were present, demonstrating their robust attachment to the fiber surface resulting from the thorough deposition and sufficient drying before epoxy treatment during preparation. After scratching the coated and beaded fibers, a “Trunk-Root” structure was observed, where the E-beads (i.e., Trunk) were clearly visible on top of the b-SWCNTs scaffold (i.e., Root) (Fig. 7 (C-D)). Here, the coating thickness was approximately 1.5  $\mu\text{m}$  (very thin) and mildly rough. This is effective for the load transfer mechanism, whereas, according to the literature, when the coating is too thick or rough, the interface is ineffective or brittle [49,50].

These observations demonstrate that the beads act as topographical anchors of the fibers in the matrix. Additionally, the coating improves the interfacial adhesion to the fiber, resulting in a more effective stress transfer from the matrix, through the beads and the impregnated CNTs, to the fibers. The plastic deformation of the matrix and the beads absorbs energy during failure, as does the pulling out of the CNTs from the impregnated matrix (Fig. 7). These effects are consistent with our experimental findings, which showed that the coated samples tended to have better fiber-bead adherence than the uncoated ones, leading to a greater withdrawal force (Fig. 6A). Simultaneously, densification

improves adhesion between SWCNTs due to increased van der Waals interactions and friction forces and improves stress transmission between individual CNTs or SWCNT bundles, resulting in more uniform load-sharing throughout the coated fiber. When a cured coated and beaded fiber is implanted in a curing matrix (same epoxy), the matrix establishes bonds with the bead surface. At the same time, a strong interface exists between the b-SWCNTs and the epoxy beads. Therefore, when both interfaces are combined in a particular fiber–matrix system, coated and beaded fibers are able to increase both interfacial shear strength and toughness.

### 3.4. b-SWCNT coating strength and toughness assessment

The following analysis provides a theoretical calculation of the coating layer strength, a sub-composite of the epoxy matrix reinforced by b-SWCNTs, using the CKT modeling approach. The CKT model assumes that the stress at the mid-plane of SWCNTs bundle, which, at failure, is the bundle strength, balances the uniform shear stress along the bundle interface, which is equal to the matrix yield strength. The calculation of the impregnated b-SWCNTs scaffold strength uses the following mixing rule:

$$\sigma_i = n_l n_0 V_c \sigma_c + V_s \sigma_s + V_m \sigma_m \quad (4)$$

where  $n_l$  and  $n_0$  are the finite length and the arbitrary spatial orientation factors, respectively.  $V_c$ ,  $V_s$ , and  $V_m$  are the volume fractions of the b-SWCNTs, surfactant, and matrix (epoxy), respectively.  $\sigma_c$ ,  $\sigma_s$ , and  $\sigma_m$  are the strength values of the b-SWCNTs, surfactant, and matrix (epoxy), respectively. The factor  $n_0$  for arbitrary orientation of the nanotubes under a 3D domain is  $n_0 = 1/5$  [51]. The finite length factor is given by

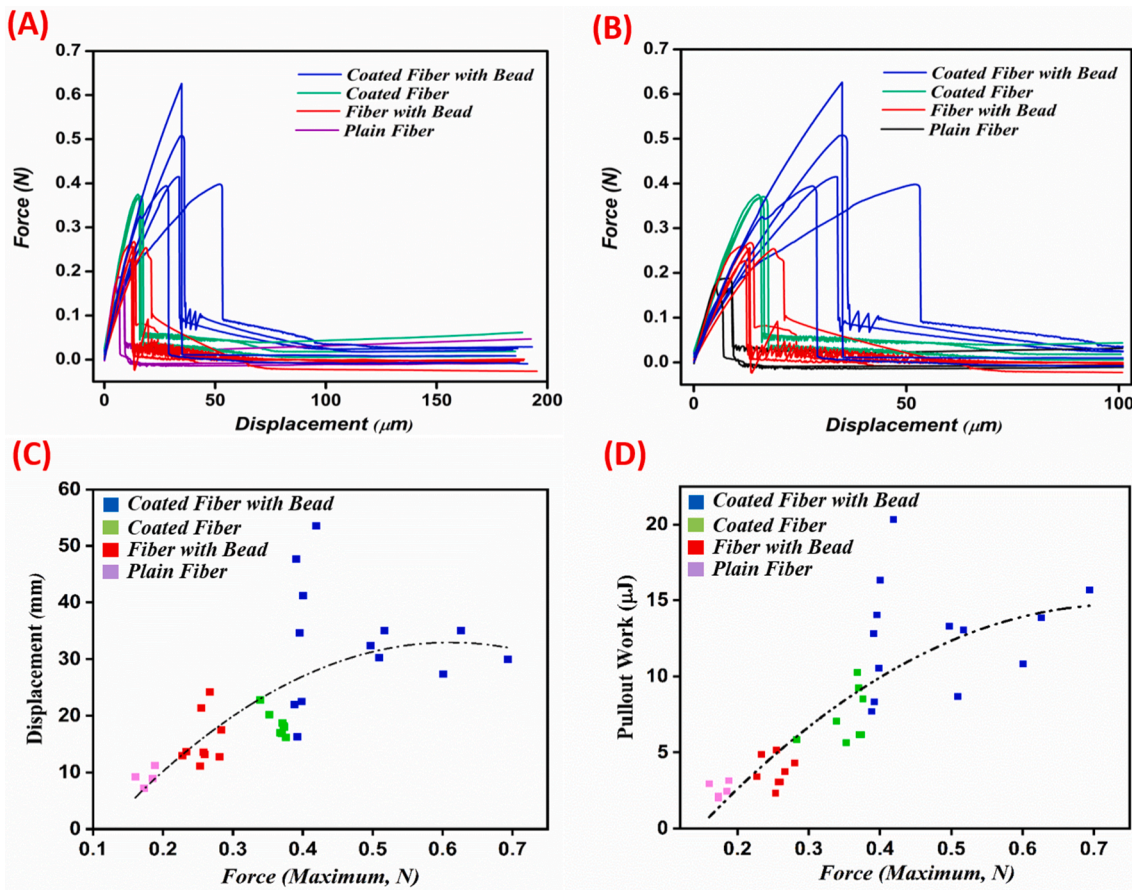


Fig. 6. Comparison of pullout characteristics of plain fibers, fibers with beads, coated fibers and coated fibers with beads; plots of (A) force vs displacement; (B) force vs displacement with a magnified elastic-plastic zone; (C) displacement vs max force; (D) Plot of pullout work vs max force.

Table 1

Measured maximum force, effective interfacial shear strength, displacement, and pullout work, during the pullout study for the different prepared micro-fibers.

Sample configuration	Force (N)	Interfacial shear strength (MPa)	Elastic-plastic displacement ( $\mu\text{m}$ )	Pullout work ( $\mu\text{J}$ )
Plain fiber	$0.18 \pm 0.01$	$34.44 \pm 2.12$	$8.76 \pm 1.67$	$2.52 \pm 0.53$
Beaded fiber	$0.26 \pm 0.02$	$48.43 \pm 3.51$	$15.59 \pm 4.48$	$4.75 \pm 2.32$
Coated fiber	$0.37 \pm 0.01$	$68.50 \pm 2.39$	$18.50 \pm 2.14$	$8.03 \pm 2.75$
Coated & beaded fiber	$0.44 \pm 0.11$	$82.71 \pm 10.63$	$32.91 \pm 8.60$	$12.72 \pm 3.56$

$n_l = \left(1 - \frac{l^b-SWCNT}{2l^b-SWCNT}\right)$  when the bundle length ( $l^b-SWCNT$ ) is longer than its critical length ( $l_c^b-SWCNT$ ), where the critical length is given by:

$$l_c^b-SWCNT = \frac{\sigma_c D_{b-SWCNT}}{2\tau_i} \quad (5)$$

Equation (4) can be reduced to [48]:

$$\sigma_t = \frac{1}{5} \left(1 - \frac{1}{2} \frac{l^b-SWCNT}{l^b-SWCNT}\right) V_c \sigma_c + V_m \sigma_m \quad (6)$$

Here, we neglected the surfactant strength ( $\sigma_s \cong 0$ ). This equation originates from the CKT-model, taking into consideration the fraction of b-SWCNTs present at the sheared interface of the fiber during the pullout test.

Lu et al. presented a range of CNT fibers strength of  $\sim 0.8$ – $1.6$  GPa [52–55]. The bundle SWCNTs used in our study are similar in structure

to CNT fibers, which are also bundles, and therefore, we selected the value of  $\sigma_c \cong 1.2$  GPa for our calculation. The average diameter of the b-SWCNTs in our study was  $D_{b-SWCNTs} = 20$  nm, and the average bundle length ( $l^b-SWCNT$ ) was  $70 \mu\text{m}$  (collected from the SEM micrographs using *ImageJ* software). The critical length ( $l_c^b-SWCNT$ ) of the bundle SWCNTs is  $0.50 \mu\text{m}$ , using equation (5) with the shear strength of the matrix + SDS + remaining gaps  $\tau_i = 23.9$  MPa ( $\sigma_m = 34.3$  MPa from Table 1, plain fiber, reduced by the relative fraction of the SDS and a final porosity of 9% (Fig. S4)). Thus, the bundle critical length is smaller than its length, and therefore equation (5) holds. The corresponding length factor ( $n_l$ ) is 0.996 on average, as only a small portion of the b-SWCNTs is pulled out from the matrix rather than broken.

Based on the weight measurements and mass densities from the TGA analysis (Fig. 8 (A & B)), we calculated the volume fractions  $V_c = 0.21$ ,  $v_s = 0.15$ , and  $V_m = 0.55$  using equations (1) and (2) (based on the porosity, see Fig. S4)). When these estimated parameters were used in equation (6), the b-SWCNTs impregnated scaffold strength ( $\sigma_t$ ) was estimated to be 67.90 MPa (using  $\sigma_m = 34.3$  MPa, Table 1). This value is very close to the effective interfacial shear strength average value for the coated fibers obtained from the pullout experiment (Table 1). The consistency of the b-SWCNT network in the scaffold and the low level of individual b-SWCNT agglomeration are validated by the similarity of these results, estimated using two different methods (the pullout test and the mixing rule).

The effective shear strength of the interface (Table 1) was evaluated directly by dividing the measured pullout force by the interfacial area of the fiber. By contrast, the tensile properties of the interface cannot be evaluated in this way, and therefore the prediction using a mixing rule was used. In isotropic homogenous materials the tensile strength is significantly higher than the shear strength; however, in fiber

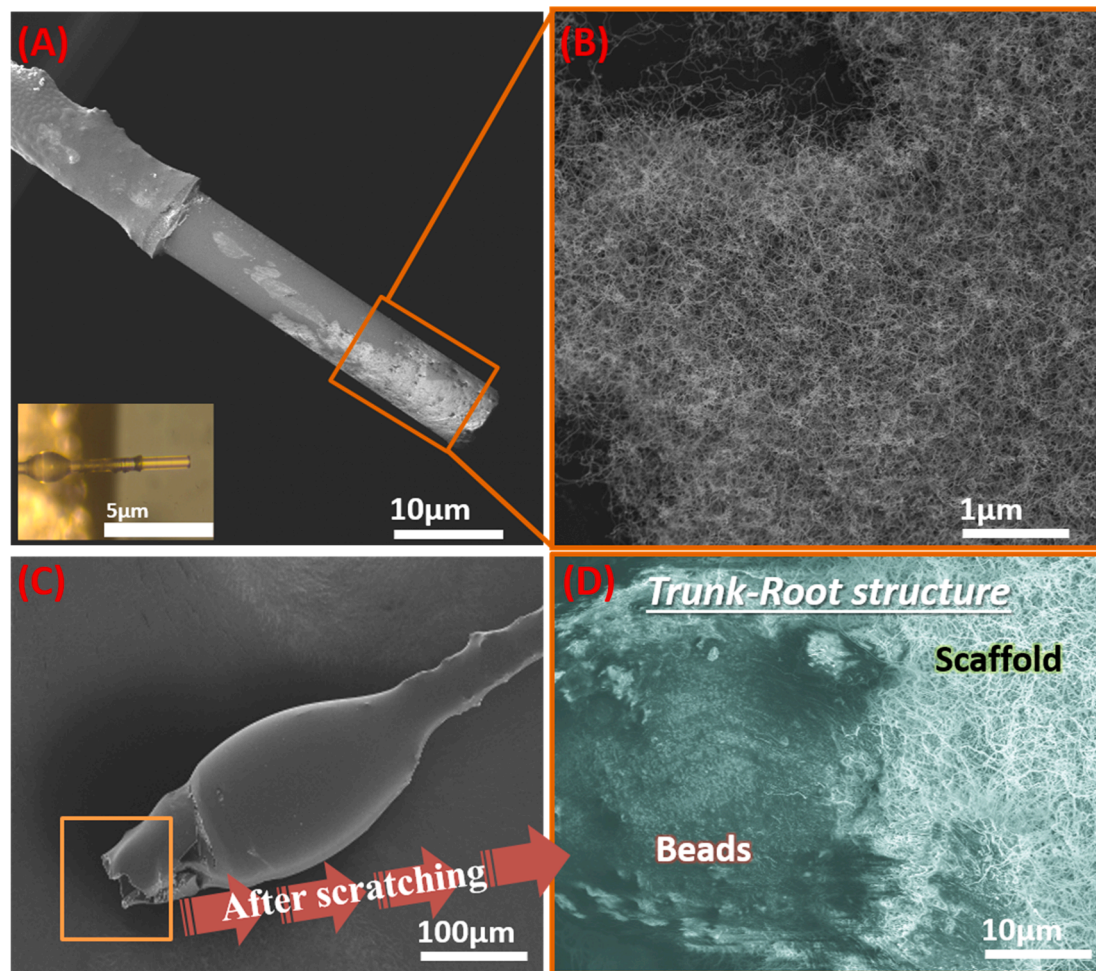


Fig. 7. (A) SEM image of a pulled-out fiber with an inset of optical visualization; (B) Magnification of the SWCNTs remaining on the pulled fiber; (C) SEM image of a single bead at the end of a coated fiber; (D) The fiber surface after scratching, displaying the “Trunk-Root” structure of a bead on top of the coating.

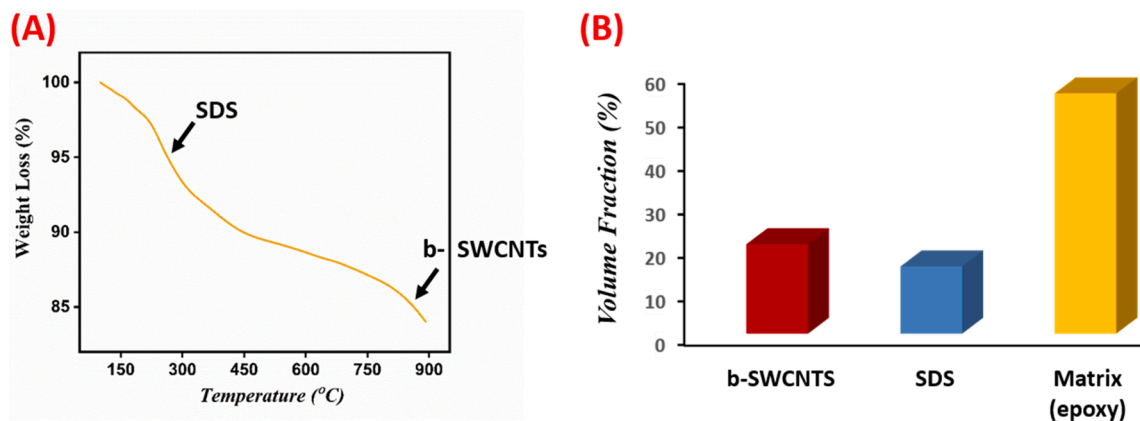
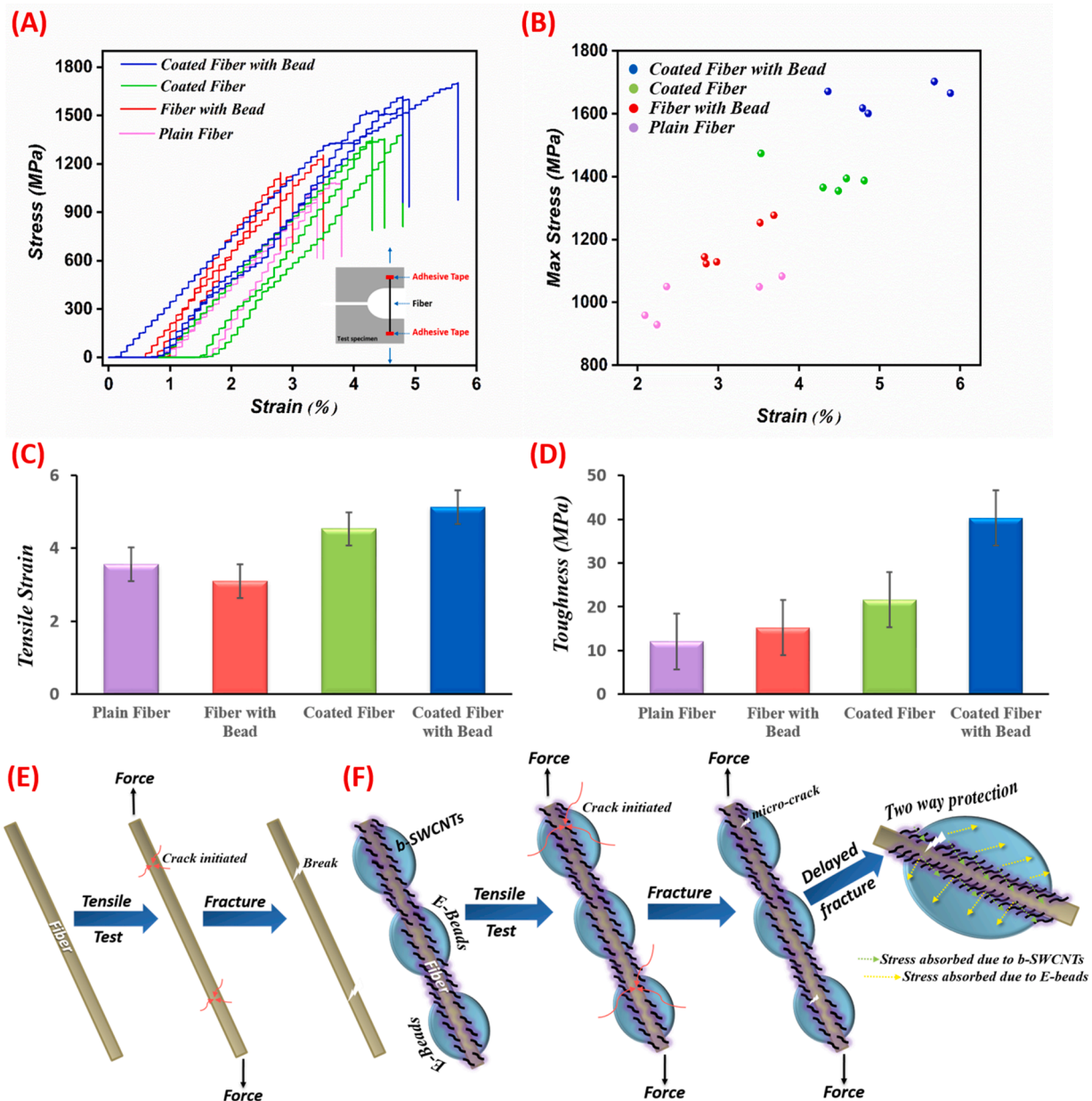


Fig. 8. (A) The b-SWCNTs scaffold TGA analysis, including the b-SWCNTs and SDS surfactant coated fibers that make up the TGA sample. Each dip in the graph represents the weight loss that occurred during heating for each material; (B) The b-SWCNT scaffold volume fraction, SDS volume fraction and matrix (epoxy) volume fraction, calculated by Equations (1) & (2).

composites, as a result of the large matrix deformation during failure, the fiber–matrix interface does not fail in pure shear but rather in a combination of shear and tension [51]. Consequently, the measured effective shear strength approaches the tensile strength of the interface, as indeed seen in our assessment.

In addition to the improvement in strength, the CNT coating enhances the toughness of the fiber–matrix interphase. Modeling the

toughness is beyond the scope of this study, but the following phenomenological simplification may apply. From Fig. 6A, we observe that the slope  $s$  of the force–displacement curve is nearly the same for the plain and coated fibers, and that the curve is fairly linear, almost up to the maximum force  $F_{max}$ . Thus, the pullout energy can be estimated by the triangular area  $G \cong \frac{1}{2}F_{max}L$ , where  $L$  is the displacement. Because of



**Fig. 9.** Tensile tests of fibers. (A) Plot of stress vs strain of the different fiber configurations; (B-D) Average max strength vs strain (%), strain and toughness of the plain fiber, fiber with multiple beads, coated fiber and coated fiber with multiple beads; Plausible mechanism of tensile fractures of (E) a pristine fiber and (F) a coated and beaded fiber.

the curve near-linearity, the displacement can be expressed by  $L \cong F_{max}/s$ , and, therefore, the pullout energy is estimated by  $G \cong \frac{1}{2}F_{max}^2/s \propto F_{max}^2$ . By comparison, the strength of the interface is proportional to the maximum force,  $\tau \propto F_{max}$  (Equation (3)). This explains why the improvement in strength due to the coating is 106 %, whereas that of the toughness is approximately 219 %, much greater due to the quadratic dependence on  $F_{max}$ .

An important question is whether the two reinforcing mechanisms used in our study, namely the coating and beading, are acting independently. This question can be addressed by the following argument. The effective interfacial strength of the pristine fiber configuration was 34.44 MPa, whereas that of the coating was 68.50 MPa, and the bead was 48.43 MPa (Equation (3) and Table 1). Thus, the net contribution of the coating was 34.06 MPa, and that of the bead was 13.99 MPa, both obtained by subtracting the value of the pristine fiber. Summing up all the individual contributions, we obtain effective interfacial strength of

about 82.5 MPa, very close to the value of the combined coated + beaded configuration in Table 1. Therefore, each mechanism contributes independently to the overall interfacial strength without affecting or degrading the other.

### 3.5. Application of coating and beading for flexible composites

So far, we have demonstrated the effectiveness of fiber coating and beading in structural composites, in which the fibers are embedded in a rigid matrix, like epoxy. In such applications, the interfacial strength of the coating and beading is of high importance for the overall composite strength. By contrast, coating and beading may be applied in other types of materials, such as flexible composites. An example is reinforced textile fabrics, in which the substrate consists of wool, cotton or polyester fibers, coated with various nanoparticles [56,57]. Another example, which is more relevant to our study, are glass fiber fabrics,

available commercially for armor, optical and encapsulation applications [58,59]. Here, we propose coating and beading of glass fibers prior to weaving the fabric, in order to increase the fabric strength and toughness, improve the binding between the fibers, and endow the fabric with functional properties, such as highly tolerable mechanical field, electrical conductivity, sensing and actuating.

Generally, interfacial strength is not as important for fabrics but rather the strength and toughness of the individual fibers that make up the fabric, as well as the fiber flexibility in bending. A detailed description is beyond the scope of this study, and therefore, we focus on the standalone fiber strength, toughness, flexibility, and electrical conductivity.

### 3.5.1. Fiber strength and toughness

To investigate the effect of CNT coating and epoxy beads on a standalone glass fiber strength, single-fiber tensile tests were conducted on pristine fibers, beaded fibers, coated fibers, and both coated and beaded fibers. The average tensile strength of the pristine fiber was  $\sim 1013$  MPa. The beaded fiber strength was  $\sim 1185$  MPa, an approximate 16 % increment compared with the pristine fiber. The strength of the b-SWCNTs coated fiber was  $\sim 1394$  MPa, whereas that of the coated and beaded fiber was  $\sim 1651$  MPa, 37 % and 63 % higher than the pristine fiber, respectively (Fig. 9A, B). In addition to the strength, the maximum strain and the toughness were improved (Fig. 9C, D), achieving simultaneous enhancement in these typically mutually exclusive parameters.

The beads, as well as the thin layer of epoxy between them (Fig. S5), have the ability to quench flaws on the fiber surfaces, improving their strength and toughness. The b-SWCNTs coating further adds to the strength and toughness. At the same time, because of the bonding and filming action of the epoxy beads, the coating scaffold was secured to the fiber surface and would not slip during the stretching process (recorded in Supporting Information Movie 2). Also, the CNTs filament-filament micro friction and adhesion to the fiber were enhanced by epoxy impregnation. The positive effect of coating and beading (which provides two-way protection) on the probability of failure, was closely analyzed by Weibull distribution (Supporting Information Section 1, Fig. S6, and Table S1), showing a narrower statistical dispersion (larger shape parameter, Fig. S6 (B-D)) compared to pristine fibers (Fig. S6A), and is illustrated schematically in Fig. 9E, F.

### 3.5.2. Fiber flexibility

When flexible composite materials are put to practical applications, they provide several advantages such as a high-strength-to-weight ratio, lower corrosion, cavitation impact, and maintenance cost, as well as improved fatigue, bending, and damping performance in the areas of aerospace, marine, high load bearing structures, sports, electronics, and the health industry. The micro-coated and beaded fibers display excellent flexibility and foldability without suffering damage or breaking when we apply stress (such as bending or rolling up), as demonstrated in digital photographs (Fig. 10). We fixed one end of the fiber with adhesive to place additional pressure on the flexibility demonstration. After coating and beading, the fibers became not only more robust mechanically, but also retained their inherent flexibility, which can meet the requirements of a wide range of potential applications.

### 3.5.3. Fiber electrical conductivity

The current–voltage characteristics of self-assembled b-SWCNTs and epoxy beaded fibers are illustrated in Fig. 11. The conductance of the coated and beaded fiber is directly linked to the b-SWCNTs deposition using the evaporation-driven technique. A possible electrical connection between the linked b-SWCNT scaffold on the glass micro-fiber surface was indicated by the increased current value, considering that the glass fibers themselves and the epoxy are not conductive. Evidently, the entrapped b-SWCNTs increased the electron flow within the coated fiber, which might act as “conducting bridges of CNTs-CNTs” on the fiber surface upon coating. It was suggested that the hopping or tunneling [60] behavior of b-SWCNTs coated on a fiber surface is the source of this electrical interaction. The current represents electron movement via b-SWCNTs in these coated fibers, where the voltage extends across the fiber surface or a fiber potential, as the conductance of these microfibers controls the current [61,62].

The micro-coated and beaded fibers exhibit a decent quantity of current up to the 2.2 mm probe location. Since the conductance of an electrical loop circuit relies on its distance, a very minimal amount of current was recorded at 4.2 mm probes distance. The enhancement in the current solely depends on b-SWCNTs connection and thickness of coatings ( $\sim 1.5$   $\mu\text{m}$  for the current study), which can be tuned by modulating the coating thickness. The probes were connected on the epoxy and beads surface and not directly to the conducting CNTs, leaving room for future improvement of the coated and beaded fibers' conductivity. Furthermore, uniaxial tension or bending of the coated and beaded fiber will induce CNTs bending, resulting in small changes in conductivity and current, making this assembly suitable for portable electronics, sensors, or transmitters. The high degree of fiber flexibility ensures that the contacts between CNTs will not break under deformation and hence will not degrade the conductivity.

## 4. Conclusions

Microscale glass fibers were treated with CNT coating and epoxy beads for the purpose of increasing their adhesive interface in a composite. Single-walled CNTs, arranged in bundles, were deposited on the fibers using evaporation-driven deposition from a solution of CNTs in acetone with an SDS surfactant, creating a uniform coating scaffold of approximately 1.5  $\mu\text{m}$  thick. Beading was achieved by applying epoxy resin on the coated fibers, implementing the Plateau-Rayleigh liquid instability. The coated and beaded fibers were embedded in an epoxy matrix and subjected to a pullout test to measure the fiber–matrix interfacial strength. Morphological and failure analyses were conducted by electron microscopy and by 3D micro-CT imaging.

The pullout tests demonstrated an improvement in the fiber–matrix interfacial shear strength of 98 % from the coating alone and 140 % by the combination of coating and beading compared to pure glass fibers. At the same time, the pullout displacement at the maximum stress was improved by 111 % and 276 %, respectively. The corresponding toughness, assessed by the total fracture energy, was improved by 219 % and 405 %, respectively. These results are substantiated by a theoretical calculation using the Cottrell-Kelly-Tyson method.

These findings imply that a composite using CNT-coated and beaded fibers should lead to significant enhancement of both strength and

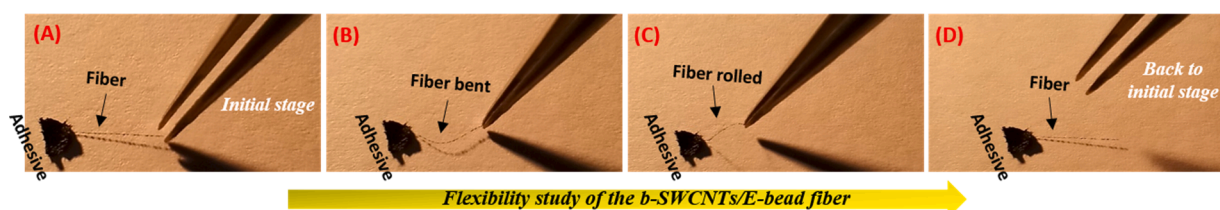


Fig. 10. (A-D) Flexibility demonstration of the micro coated and beaded fibers with ultra-vision digital photographs.

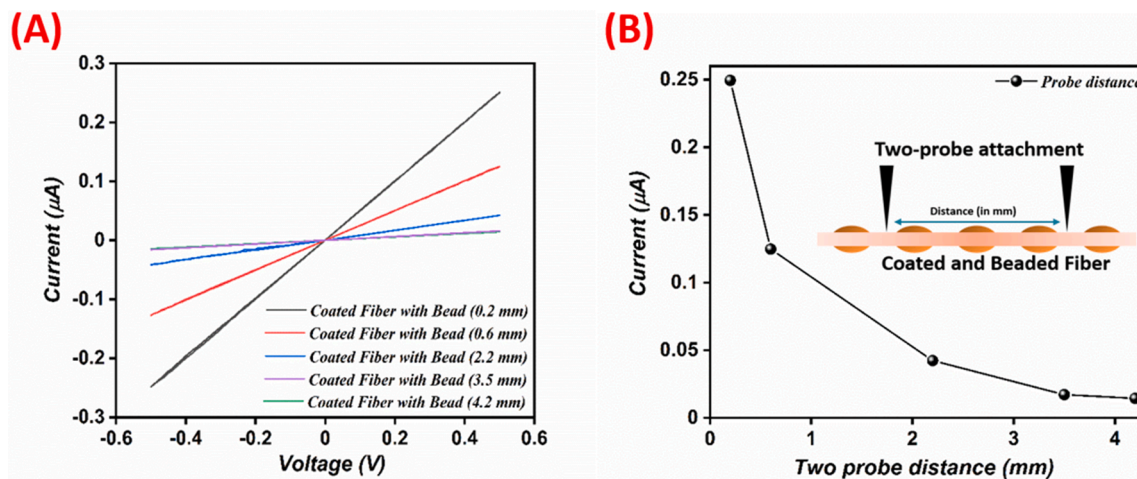


Fig. 11. (A) Current-Voltage (I-V) plot of a coated fiber with beads under different probe distances; (B) Plot of current vs two-probe distance.

toughness simultaneously, properties that are typically mutually exclusive. This is achieved by the combination of strengthening the interface between the fibers and the matrix using the CNT-deposited and epoxy-impregnated scaffold, together with the topological anchoring action of the beads. The properties of the coated and beaded fibers can be tuned for different applications by modifying the dimensions of the CNT bundles used in the coating and the size of the beads.

Coated and beaded fibers may also be implemented in flexible composites, by weaving them into the fabric. In such applications, the strength and toughness of the standalone fiber are considered. A tensile test conducted on standalone coated and beaded fibers demonstrated a significant improvement of 63 % in strength, as well as an improvement in the maximum strain. Weibull analysis showed that the strength distribution in the coated and beaded fibers is narrower than the pristine fibers, indicating the quenching of defects by this treatment. These fibers were also tested for mechanical flexibility and electrical conductivity, making them good candidates for ultra-lightweight and flexible functional composites suitable for micro-electronics materials and sensors.

#### CRedit authorship contribution statement

**Sabyasachi Ghosh:** Conceptualization, Methodology, Investigation, Data curation, Writing – original draft, Formal analysis, Software, Validation. **Israel Greenfeld:** Methodology, Investigation, Data curation, Software. **H. Daniel Wagner:** Conceptualization, Supervision, Writing – review & editing, Funding acquisition.

#### Declaration of Competing Interest

The authors declare that they have no known competing financial interests or personal relationships that could have appeared to influence the work reported in this paper.

#### Data availability

Data will be made available on request.

#### Acknowledgement

The authors would like to acknowledge support from the G.M.J. Schmidt Minerva Centre of Supramolecular Architectures at the Weizmann Institute, and the generosity of the Harold Perlman family. HDW is the incumbent of the Livio Norzi Professorial Chair in Materials Science. SG wants to thank Dr. Vlad Brumfeld (Scientific advisor, Weizmann Institute) and Dr. Sudipta Bera (MCMS, Weizmann Institute) for the micro-CT scanning analysis and conductivity measurements. This

research was supported in part by the Israel Science Foundation (ISF grant #2439/19).

#### Appendix A. Supplementary material

Supplementary data to this article can be found online at <https://doi.org/10.1016/j.compositesa.2023.107427>.

#### References

- [1] Wang J, Luo X, Wu T, Chen Y. High-strength carbon nanotube fibre-like ribbon with high ductility and high electrical conductivity. *Nat Commun* 2014;5(1):1–8.
- [2] Liu LQ, Tasis D, Prato M, Wagner HD. Tensile mechanics of electrospun multiwalled nanotube/poly (methyl methacrylate) nanofibers. *Adv Mater* 2007;19(9):1228–33.
- [3] Idarraga G, Jalalvand M, Fotouhi M, Meza J, Wisnom MR. Gradual failure in high-performance unidirectional thin-ply carbon/glass hybrid composites under bending. *Compos Struct* 2021;271:114128.
- [4] Ghosh S, Nitin B, Remanan S, Bhattacharjee Y, Ghorai A, Dey T, et al. A multifunctional smart textile derived from merino wool/nylon polymer nanocomposites as next generation microwave absorber and soft touch sensor. *ACS Appl Mater Interfaces* 2020;12(15):17988–8001.
- [5] Ritchie RO. The conflicts between strength and toughness. *Nat Mater* 2011;10(11):817–22.
- [6] Ray BC, Rathore D. Durability and integrity studies of environmentally conditioned interfaces in fibrous polymeric composites: Critical concepts and comments. *Adv Colloid Interface Sci* 2014;209:68–83.
- [7] Wong DW, Zhang H, Bilotti E, Peijs T. Interlaminar toughening of woven fabric carbon/epoxy composite laminates using hybrid aramid/phenoxy interleaves. *Compos A Appl Sci Manuf* 2017;101:151–9.
- [8] Rev T, Wisnom MR, Xu X, Czél G. The effect of transverse compressive stresses on tensile failure of carbon fibre/epoxy composites. *Compos A Appl Sci Manuf* 2022;156:106894.
- [9] Veedu VP, Cao A, Li X, Ma K, Soldano C, Kar S, et al. Multifunctional composites using reinforced laminae with carbon-nanotube forests. *Nat Mater* 2006;5(6):457–62.
- [10] Wagner HD. Hierarchical Interfaces as Fracture Propagation Traps in Natural Layered Composites. *Materials* 2021;14(22):6855.
- [11] Greenfeld I, Rodricks CW, Sui X, Wagner HD. Beaded fiber composites—Stiffness and strength modeling. *J Mech Phys Solids* 2019;125:384–400.
- [12] Choi M, Jeon B, Chung LJ. The effect of coupling agent on electrical and mechanical properties of carbon fiber/phenolic resin composites. *Polymer* 2000;41(9):3243–52.
- [13] Arslan C, Dogan M. The effects of silane coupling agents on the mechanical properties of basalt fiber reinforced poly (butylene terephthalate) composites. *Compos B Eng* 2018;146:145–54.
- [14] Wang D, Xuan L, Han G, Wong AH, Wang Q, Cheng W. Preparation and characterization of foamed wheat straw fiber/polypropylene composites based on modified nano-TiO<sub>2</sub> particles. *Compos A Appl Sci Manuf* 2020;128:105674.
- [15] Iijima S. Helical microtubules of graphitic carbon. *Nature* 1991;354(6348):56–8.
- [16] Yu M-F, Lourie O, Dyer MJ, Moloni K, Kelly TF, Ruoff RS. Strength and breaking mechanism of multiwalled carbon nanotubes under tensile load. *Science* 2000;287(5453):637–40.
- [17] Liu H, Nishide D, Tanaka T, Kataura H. Large-scale single-chirality separation of single-wall carbon nanotubes by simple gel chromatography. *Nat Commun* 2011;2(1):1–8.

- [18] Barber A, Kaplan-Ashiri I, Cohen S, Tenne R, Wagner HD. Stochastic strength of nanotubes: an appraisal of available data. *Compos Sci Technol* 2005;65(15–16):2380–4.
- [19] Barber AH, Andrews R, Schadler LS, Wagner HD. On the tensile strength distribution of multiwalled carbon nanotubes. *Appl Phys Lett* 2005;87(20):203106.
- [20] Tzounis L, Zappalorto M, Panozzo F, Tsirka K, Maragoni L, Paipetis AS, et al. Highly conductive ultra-sensitive SWCNT-coated glass fiber reinforcements for laminate composites structural health monitoring. *Compos B Eng* 2019;169:37–44.
- [21] Wichmann MH, Sumfleth J, Gojny FH, Quaresimin M, Fiedler B, Schulte K. Glass-fibre-reinforced composites with enhanced mechanical and electrical properties—benefits and limitations of a nanoparticle modified matrix. *Eng Fract Mech* 2006;73(16):2346–59.
- [22] Mirabedini A, Ang A, Nikzad M, Fox B, Lau KT, Hameed N. Evolving strategies for producing multiscale graphene-enhanced fiber-reinforced polymer composites for smart structural applications. *Adv Sci* 2020;7(11):1903501.
- [23] Cao C, Lin Z, Liu X, Jia Y, Saiz E, Wolf SE, et al. Strong reduced graphene oxide coated bombyx mori silk. *Adv Funct Mater* 2021;31(34):2102923.
- [24] Kaplan-Ashiri I, Cohen SR, Gartsman K, Ivanovskaya V, Heine T, Seifert G, et al. On the mechanical behavior of WS<sub>2</sub> nanotubes under axial tension and compression. *Proceedings of the National Academy of Sciences*. 2006; 103(3): 523–8.
- [25] Kamae T, Drzal LT. Carbon Fiber/Epoxy Composite Property Enhancement through Incorporation of Carbon Nanotubes at the Fiber-Matrix Interphase-Part II: Mechanical and Electrical Properties of Carbon Nanotube Coated Carbon Fiber Composites. *Compos Part A: Appl Sci Manuf* 2022;107023.
- [26] Wang W, Xian G, Li H. Surface modification of ramie fibers with silanized CNTs through a simple spray-coating method. *Cellul* 2019;26(13):8165–78.
- [27] Zhang J, Zhuang R, Liu J, Mäder E, Heinrich G, Gao S. Functional interphases with multi-walled carbon nanotubes in glass fiber/epoxy composites. *Carbon* 2010;48(8):2273–81.
- [28] Lee JU, Park B, Kim B-S, Bae D-R, Lee W. Electrophoretic deposition of aramid nanofibers on carbon fibers for highly enhanced interfacial adhesion at low content. *Compos A Appl Sci Manuf* 2016;84:482–9.
- [29] Hung P-y, Lau K-t, Fox B, Hameed N, Lee JH, Hui D. Surface modification of carbon fibre using graphene-related materials for multifunctional composites. *Compos B Eng* 2018;133:240–57.
- [30] An Q, Rider AN, Thostenson ET. Electrophoretic deposition of carbon nanotubes onto carbon-fiber fabric for production of carbon/epoxy composites with improved mechanical properties. *Carbon* 2012;50(11):4130–43.
- [31] Si G, Zhuang RC, Zhang J, Liu JW, Mäder E. Glass fibers with carbon nanotube networks as multifunctional sensors. *Adv Funct Mater* 2010;20(12):1885–93.
- [32] Yildiz K, Gürkan İ, Turgut F, Cebeci FÇ, Cebeci H. Fracture toughness enhancement of fuzzy CNT-glass fiber reinforced composites with a combined reinforcing strategy. *Compos Commun* 2020;21:100423.
- [33] Vilatela JJ, Khare R, Windle AH. The hierarchical structure and properties of multifunctional carbon nanotube fibre composites. *Carbon* 2012;50(3):1227–34.
- [34] Azarniya A, Azarniya A, Sovizi S, Hosseini HRM, Varol T, Kawasaki A, et al. Physicomechanical properties of spark plasma sintered carbon nanotube-reinforced metal matrix nanocomposites. *Prog Mater Sci* 2017;90:276–324.
- [35] Duong HM, Gong F, Liu P, Tran TQ. Advanced fabrication and properties of aligned carbon nanotube composites: Experiments and modeling. *Carbon nanotubes—current progress of their polymer composites*. 2016.
- [36] Nie X, Cui J, Jiang W. Ultralong cylindrical micelles precisely located with semiconductor nanorods by solvent evaporation-driven self-assembly. *Soft Matter* 2014;10(40):8051–9.
- [37] Nissenbaum A, Greenfeld I, Wagner H. Evaporation-driven 3D CNT scaffolding for composite reinforcement. *Carbon* 2021;173:705–14.
- [38] Rodricks CW, Greenfeld I, Wagner HD. Polymer beads as interfacial obstacles in fibre composites. *Compos Sci Technol* 2021;210:108793.
- [39] Rodricks CW, Greenfeld I, Fiedler B, Wagner HD. Fragmentation of Beaded Fibres in a Composite. *Materials* 2022;15(3):890.
- [40] Cottrell AH. Strong solids. *Proc Roy Soc London Series A Math Phys Sci* 1964; 282 (1388): 2–9.
- [41] Kelly A. Interface effects and the work of fracture of a fibrous composite. *Proc Roy Soc London A Math Phys Sci* 1970;319(1536):95–116.
- [42] Kelly A, Tyson WR. Tensile properties of fibre-reinforced metals: copper/tungsten and copper/molybdenum. *J Mech Phys Solids* 1965;13(6):329–50.
- [43] Misra A, Raney J, Craig A, Daraio C. Effect of density variation and non-covalent functionalization on the compressive behavior of carbon nanotube arrays. *Nanotechnology* 2011;22(42):425705.
- [44] Tummala NR, Striolo A. SDS surfactants on carbon nanotubes: aggregate morphology. *ACS Nano* 2009;3(3):595–602.
- [45] Vaisman L, Wagner HD, Marom G. The role of surfactants in dispersion of carbon nanotubes. *Adv Colloid Interface Sci* 2006;128:37–46.
- [46] Miller B, Muri P, Rebenfeld L. A microbond method for determination of the shear strength of a fiber/resin interface. *Compos Sci Technol* 1987;28(1):17–32.
- [47] Mehan M, Schadler L. Micromechanical behavior of short-fiber polymer composites. *Compos Sci Technol* 2000;60(7):1013–26.
- [48] Greenfeld I, Wagner HD. Nanocomposite toughness, strength and stiffness: role of filler geometry. *Nanocomposites* 2015;1(1):3–17.
- [49] Godara A, Gorbatiikh L, Kalinka G, Warriar A, Rochez O, Mezzo L, et al. Interfacial shear strength of a glass fiber/epoxy bonding in composites modified with carbon nanotubes. *Compos Sci Technol* 2010;70(9):1346–52.
- [50] Yu B, Jiang Z, Tang X-Z, Yue CY, Yang J. Enhanced interphase between epoxy matrix and carbon fiber with carbon nanotube-modified silane coating. *Compos Sci Technol* 2014;99:131–40.
- [51] Piggott M. Load bearing fibre composites. Springer Science & Business Media; 2002.
- [52] Lu W, Zu M, Byun JH, Kim BS, Chou TW. State of the art of carbon nanotube fibers: opportunities and challenges. *Adv Mater* 2012;24(14):1805–33.
- [53] Zu M, Li Q, Zhu Y, Dey M, Wang G, Lu W, et al. The effective interfacial shear strength of carbon nanotube fibers in an epoxy matrix characterized by a microdroplet test. *Carbon* 2012;50(3):1271–9.
- [54] Zhu H, Xu C, Wu D, Wei B, Vajtai R, Ajayan P. Direct synthesis of long single-walled carbon nanotube strands. *Science* 2002;296(5569):884–6.
- [55] Behabtu N, Green MJ, Pasquali M. Carbon nanotube-based neat fibers. *Nano Today* 2008;3(5–6):24–34.
- [56] Ghosh S, Remanan S, Mondal S, Ganguly S, Das P, Singha N, et al. An approach to prepare mechanically robust full IPN strengthened conductive cotton fabric for high strain tolerant electromagnetic interference shielding. *Chem Eng J* 2018;344:138–54.
- [57] Ghosh S, Ganguly S, Das P, Das TK, Bose M, Singha NK, et al. Fabrication of reduced graphene oxide/silver nanoparticles decorated conductive cotton fabric for high performing electromagnetic interference shielding and antibacterial application. *Fibers Polym* 2019;20(6):1161–71.
- [58] Boufaida Z, Farge L, André S, Meshaka Y. Influence of the fiber/matrix strength on the mechanical properties of a glass fiber/thermoplastic-matrix plain weave fabric composite. *Compos A Appl Sci Manuf* 2015;75:28–38.
- [59] Zhao L, Yu Y, Huang H, Yin X, Peng J, Sun J, et al. High-performance polyphenylene sulfide composites with ultra-high content of glass fiber fabrics. *Compos B Eng* 2019;174:106790.
- [60] Ghosh S, Ganguly S, Maruthi A, Jana S, Remanan S, Das P, et al. Micro-computed tomography enhanced cross-linked carboxylated acrylonitrile butadiene rubber with the decoration of new generation conductive carbon black for high strain tolerant electromagnetic wave absorber. *Mater Today Commun* 2020;24:100989.
- [61] Collins PG, Bando H, Zettl A. Nanoscale electronic devices on carbon nanotubes. *Nanotechnology* 1998;9(3):153.
- [62] Yang K, Zhang F, Chen Y, Zhang H, Xiong B, Chen H. Recent progress on carbon-based composites in multidimensional applications. *Compos A Appl Sci Manuf* 2022;157:106906.